Solid State Ionics 14 (1984) 205–216
North-Holland, Amsterdam

THE THERMODYNAMIC AND THERMOELECTRIC PROPERTIES OF Li_xTiS_2 AND Li_xCoO_2

A. HONDERS, J.M. der KINDEREN, A.H. van HEEREN,
J.H.W. de WIT and G.H.J. BROERS
Inorganic Chemistry Department, State University of Utrecht, Croesestraat 77A, 3522AD Utrecht, The Netherlands

Received 25 May 1984

The partial thermodynamic functions $\Delta\bar{H}_{Li}$ and $\Delta\bar{S}_{Li}$ for $Li_xTi_{1.03}S_2$ ($0.13 \leqslant x \leqslant 0.97$) and $Li_{0.95}CoO_2$ were obtained from EMF-temperature measurements ($T = -30$–$20°C$). For $Li_xTi_{1.03}S_2$, the x-dependence of these quantities is discussed in relation to a semiempirical expression for the EMF–x relation. The electronic component of the thermoelectric power in $Li_xTi_{1.03}S_2$ ($0 \leqslant x \leqslant 0.97$, $T = 50$–$200°C$) and Li_xCoO_2 ($0.20 \leqslant x \leqslant 1.00$, $T = 30$–$400°C$) was determined. From the sign of the (electronic) Seebeck coefficient it followed that $Li_xTi_{1.03}S_2$ is a n-type and Li_xCoO_2 a p-type electronic conductor. The influence of the amount of inserted lithium and temperature dependence on the Seebeck coefficient is discussed. A new method to determine the ionic heat of transport directly from the ionic Seebeck coefficient was developed. This method was applied to $Li_xTi_{1.03}S_2$ ($0.61 \leqslant x \leqslant 0.97$, $T = -30$–$30°C$). The heat of transport is much smaller than the activation enthalpy for Li^+-conduction, indicating a high ionic polaron binding energy. Thermogravimetric analysis indicates that Li_xCoO_2 with $x < 1$ decomposes to Li_1CoO_2 and Co_2O_3 at temperatures higher than 80°C. This is sustained by the data for the electronic Seebeck coefficient. Also the thermodynamic, thermoelectric and kinetic data of $Li_xTi_{1.03}S_2$ are critically compared with those of Ag_xTiS_2.

1. Introduction

In recent years considerable attention has been paid to the chemical and physical properties of insertion compounds, because of their potential application as cathode materials in secondary battery systems [1–3]. Up to now only a limited amount of data on the partial thermodynamic functions ($\Delta\bar{H}_M$, $\Delta\bar{S}_M$ the partial enthalpy and entropy of dissolution of the metal M in the M_xSSE) is available. Dudley et al. [4] have determined $\Delta\bar{H}_{Cu}$ and $\Delta\bar{S}_{Cu}$ for $Cu_xMo_6S_{8-y}$ ($0 < x < 3.5$), while Scholtens et al. [5] and Honders et al. [6] have shown that silver insertion compounds have remarkable thermodynamic properties. We therefore determined $\Delta\bar{H}_{Li}$ and $\Delta\bar{S}_{Li}$ in $Li_xTi_{1.03}S_2$ from EMF-temperature measurements on the cells: $Li/1M\text{-}LiClO_4$ in propylene carbonate/$Li_xTi_{1.03}S_2$ $0.13 \leqslant x \leqslant 0.97$ $T = -20$–$20°C$. The x-dependence of these quantities is discussed in relation to the semiempirical expression for the EMF–x relation of the Li/Li_xTiS_2 cell, proposed by Armand [7].

In addition to previous papers [6,8,9] on the electronic and ionic component of the thermoelectric power in Ag_xTiS_2 and Ag_xNiPS_3, we now report on thermoelectric power measurements on $Li_xTi_{1.03}S_2$ and Li_xCoO_2. The electronic component of the thermoelectric power was determined in the thermo cells:

$$Pt\,|\,Li_xTi_{1.03}S_2\,|\,Pt \qquad 0.13 \leqslant x \leqslant 0.97\,, \qquad T = 50\text{–}200°C\,,$$

$$Au\,|\,Li_xCoO_2\,|\,Au \qquad 0.20 \leqslant x \leqslant 1.00\,, \qquad T = 30\text{–}400°C\,.$$
$$(T) \qquad (T+\Delta T)$$

From the sign of the (electronic) Seebeck coefficient the sign of the mobile electronic charge carriers can be deduced, while the absolute value of the Seebeck coefficient is a measure for the carrier density in these materials. The influence of the amount of inserted lithium and temperature on the carrier density is discussed.

In a similar way as for Ag_xTiS_2 and Ag_xNiPS_3 [6,9] we determined the ionic component of the thermoelectric power in $Li_xTi_{1.03}S_2$ in thermo cells of the type:

$$Pt|Li|electrolyte|Li_xTi_{1.03}S_2|electrolyte|Li|Pt,$$

$$(\longleftarrow T \longrightarrow) \qquad (\longleftarrow T + \Delta T \longrightarrow)$$

electrolyte = 1 M·$LiClO_4$ in propylene carbonate soaked onto glass-fibre paper, $0.61 \leqslant x \leqslant 0.97$, $T = -30$–$30°C$. Because the results were only poorly reproducible we used an alternative cell array to determine the ionic component of the thermoelectric power:

$$Pt|Li_xTi_{1.03}S_2|electrolyte|Li_xTi_{1.03}S_2|$$

$$(\longleftarrow T \longrightarrow)$$

$$electrolyte|Li_xTi_{1.03}S_2|Pt$$

$$(\longleftarrow T + \Delta T \longrightarrow)$$

The advantage of this novel approach is that the ionic heat of transport ($Q^*_{Li^+}$) can be determined directly from the Seebeck coefficient. Like for Ag_xTiS_2 and Ag_xNiPS_3 [6,9], the "extended lattice gas model" of Girvin [10] is used to explain the observed difference between the values for $Q^*_{Li^+}$ and the activation enthalpy for Li^+-conduction.

From recent studies on Li^+-ion diffusion in Li_xCoO_2 [11] it followed that the Li_xCoO_2 materials with $x < 1$ are unstable. Because the decomposition process is slow at room temperature, we performed thermogravimetric analysis (TGA) in the temperature range 20–1050°C. The TGA results are discussed together with the data for the electronic Seebeck coefficient.

2. Experimental

The synthesis and characterization of the $Li_xTi_{1.03}S_2$ and Li_xCoO_2 materials have been discussed in a previous paper [11].

The EMF-temperature behaviour of $Li_xTi_{1.03}S_2$ was studied for both chemically and electrochemically synthesized materials, using pellets with a diameter of 0.8 cm and a thickness of 1 mm. Pellets of chemically synthesized $Li_xTi_{1.03}S_2$ with $x < 0.61$ crumbled off in contact with the electrolyte (1 M·$LiClO_4$ in propylene carbonate), and could therefore not be used for our experiments. The EMF-temperature measurements were completely reproducible in both cooling and heating direction.

The electronic and ionic component of the thermoelectric power in $Li_xTi_{1.03}S_2$ were measured for chemically synthesized materials. The $Li_xTi_{1.03}S_2$ pellets had a diameter of 0.6 cm and a length of $\simeq$1.5 cm; the apparent densities were in the order of 65–80% of the theoretical density [9]. The ionic probes (Li|electrolyte, $Li_xTi_{1.03}S_2$|electrolyte), which were used for the measurement of the ionic component of the thermoelectric power, had a thickness of 1–2 mm. The electrolyte was a 1 M·$LiClO_4$ solution in propylene carbonate, that was soaked onto Whatmann GF/D glass-fibre paper.

The Li_xCoO_2 samples with x = 0.80, 0.60 and 0.20, which were used for the measurement of the electronic component of the thermoelectric power, were prepared by electrochemical desintercalation of Li_1CoO_2 pellets, using a current of 30 μA. Because the amounts of the Li_1CoO_2 starting material were relatively large, this procedure lasted several months. The pellets were then thoroughly washed with propylene carbonate and 2-methyltetrahydrofuran, and dried under vacuum. The Li_xCoO_2 pellets had a diameter of 0.6 cm and a length of $\simeq$0.5 cm; the apparent densities were $\simeq$80% of the theoretical density. The chemical composition of the Li_xCoO_2 materials was determined with flame emission spectroscopy for the lithium content, and atomic absorption spectroscopy for the cobalt content. The results were in good agreement with expected values from the coulometric titrations.

Thermogravimetric analysis (TGA) and differential thermal analysis (DTA) of electrochemically synthesized Li_xCoO_2 materials with $0.16 \leqslant x \leqslant 1.00$ were performed with a Mettler TA 2000 thermobalance, in dry oxygen. All the other experimental procedures and the equipment used, have been described in previous papers [8,11,12].

3. The thermodynamics of insertion compounds

3.1. Theory

The aim of this section is to derive some simple equations describing the dependence on x and temperature of the relevant thermodynamic quantities of insertion compounds. The basic thermodynamic equations for a M/M_xSSE cell are:

$$\mathrm{EMF}(x,T) = -\Delta\bar{G}_M(x,T)/F$$

$$= F^{-1}\left[-\Delta\bar{H}_M(x,T) + T\Delta\bar{S}_M(x,T)\right], \quad (1)$$

$$\Delta\bar{S}_M/F = \partial\mathrm{EMF}/\partial T, \quad (2)$$

$$-\Delta\bar{H}_M/F = \mathrm{EMF} - T(\partial\mathrm{EMF}/\partial T), \quad (3)$$

where

$$\Delta\bar{S}_M = \bar{S}_{M^+}(x,T) - S^0_M(T), \quad (4)$$

$$\Delta\bar{H}_M = \bar{H}_{M^+}(x,T) - H^0_M(T). \quad (5)$$

$\Delta\bar{G}_M$, $\Delta\bar{S}_M$ and $\Delta\bar{H}_M$ are the partial Gibbs free energy, entropy and enthalpy of dissolution of the metal M in the M_xSSE, respectively. $\bar{S}_{M^+}$ and $\bar{H}_{M^+}$ are the partial entropy and enthalpy of the M^+-ions in the M_xSSE; S^0_M and H^0_M are the standard entropy and enthalpy of the metal M.

A semiempirical expression for the EMF–x relation of a M/M_xSSE cell is given by [7]:

$$\mathrm{EMF}(x,T) = E^0(T) - RT/F\ln(1-x)^{-1}$$

$$-(RT/F)g(T)[x-\tfrac{1}{2}], \quad (6)$$

where $E^0(T)$ is the EMF for the standard condition $x = \frac{1}{2}$, and $g(T)$ is a factor accounting for the repulsion between the M^+-ions in the M_xSSE. From the combination of eqs. (2) and (3) with eq. (6), it follows that

$$\Delta\bar{S}_M = \Delta\bar{S}^0_M - R\ln x/(1-x) - Rg[x-\tfrac{1}{2}]$$

$$-RT[x-\tfrac{1}{2}]\partial g/\partial T, \quad (7)$$

$$\Delta\bar{H}_M = \Delta\bar{H}^0_M + R[x-\tfrac{1}{2}]\,\partial g/\partial(T^{-1}), \quad (8)$$

where

$$\Delta\bar{S}^0_M = F\partial E^0/\partial T, \quad (9)$$

$$\Delta\bar{H}^0_M = -F[E^0 - T\partial E^0/\partial T]. \quad (10)$$

The relation between the thermodynamic factor (K_t) and the g-factor is given by [11,13]:

$$K_t \equiv \partial\ln a/\partial\ln c = -(F/RT)\,\partial\,\mathrm{EMF}/\partial\ln x$$

$$= 1 + x/(1-x) + gx, \quad (11)$$

$$\partial K_t/\partial(T^{-1}) = x[\partial g/\partial(T^{-1})], \quad (12)$$

where a is the activity and c the concentration of the M^+-ions in the M_xSSE. In the next section (3.2) these equations will be used for the $Li/Li_xTi_{1.03}S_2$ cell.

3.2. Results and discussion

EMF-temperature measurements were performed on the cells:

$Li/1\ M{\cdot}LiClO_4$ in propylene carbonate/$Li_xTi_{1.03}S_2$

$$0.13 \leqslant x \leqslant 0.97, \quad (I)$$

$Li/1\ M{\cdot}LiClO_4$ in propylene carbonate/$Li_{0.95}CoO_2$ (II)

in the temperature range –30–20°C. Some typical EMF–T curves are shown in fig. 1. The EMF has a negative temperature coefficient, and $\Delta\bar{G}_{Li}$ almost equals $\Delta\bar{H}_{Li}$ (see also table 1). For $Li_xTi_{1.03}S_2$, this

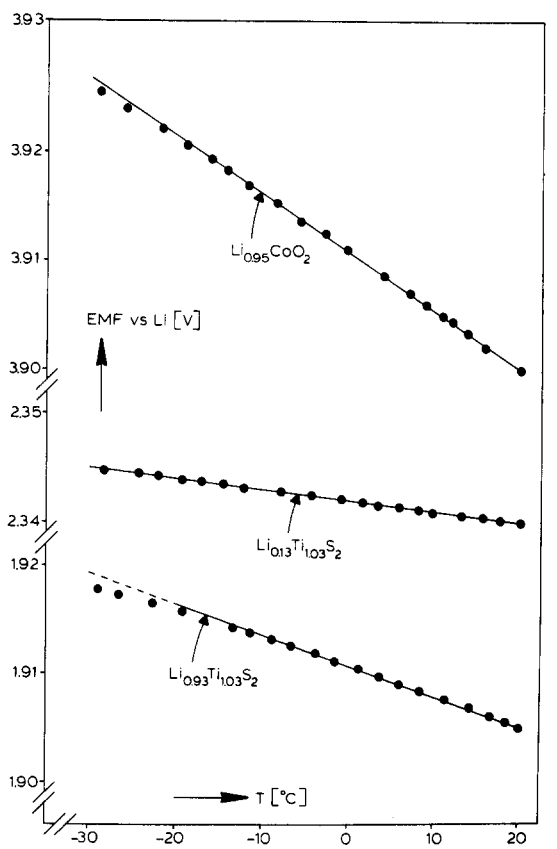

Fig. 1. EMF-temperature behaviour of the $Li/Li_xTi_{1.03}S_2$ and $Li/Li_{0.95}CoO_2$ cells.

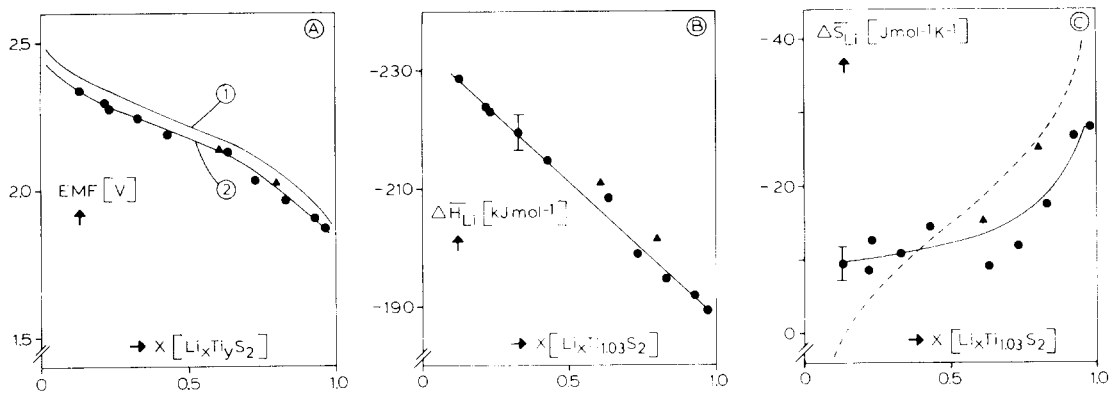

Fig. 2. Compositional variation with x of the partial enthalpy (fig. B) and entropy (fig. C) of dissolution of lithium in $Li_xTi_{1.03}S_2$, for chemically (▲) and electrochemically (●) synthesized materials. In fig. A the EMF of the $Li/Li_xTi_yS_2$ cell at 20°C is depicted – curve 1: $y = 1.01$, ref. [14]; curve 2: $y = 1.03$, this work. The dashed line in fig. C represents $\Delta\bar{S}_{Li}$ as calculated from eq. (14) for $\Delta S^0_{Li} = 15$ J mol^{-1} K^{-1}.

behaviour is observed throughout the whole x-range. In fig. 2, $\Delta\bar{H}_{Li}$ and $\Delta\bar{S}_{Li}$ for $Li_xTi_{1.03}S_2$, as determined from the EMF–T curves, are shown. $|\Delta\bar{H}_{Li}|$ decreases and $|\Delta\bar{S}_{Li}|$ increases with increasing x. Qualitatively, this is in accordance with the model as described in section 3.1: filling up the Van der Waals gap of TiS_2 with Li results in an increasing influence of the repulsion term, leading to an increasing (in positive direction) $\bar{H}_{Li^+}$; while the decreasing number of available Li-sites results in a decreasing $\bar{S}_{Li^+}$. Quantitatively, because the EMF–T curves are straight lines, $\Delta\bar{H}^0_{Li}$, $\Delta\bar{H}_{Li}$, $\Delta\bar{S}^0_{Li}$ and $\Delta\bar{S}_{Li}$ are virtually temperature independent in the relevant temperature range. Also, because $\Delta\bar{H}_{Li}$ varies linearly with x (see fig. 2b) the temperature dependence of the g-factor can be described by:

$$g(T) = \alpha/T\,, \tag{13}$$

where α is a numerical constant. Consequently, eq. (7) reduces to

$$\Delta\bar{S}_{Li} = \Delta\bar{S}^0_{Li} - R \ln x/(1-x)\,. \tag{14}$$

From the slope of the $\Delta\bar{H}_{Li}$ versus x curve (see fig. 2b) it follows that $\partial g/\partial(T^{-1}) = 5.53 \times 10^3$ K for $0.13 \leqslant x \leqslant 0.97$, according to eq. (8). The positive sign indicates that the thermodynamic factor increases with decreasing temperature, according to eq. (12). This follows also from basic thermodynamic considerations: as the thermodynamic factor is a measure for the ideality of the "solution" of Li in TiS_2, this "solution" is expected to behave more ideally for higher temperatures. For $Li_{0.80}Ti_{1.03}S_2$ we determined the thermodynamic factor (directly) from the EMF–x curves at different temperatures. The results are shown in fig. 3, from which it follows that $\partial K_t/\partial(T^{-1}) = 4.40 \times 10^3$ K $\simeq 0.8\ \partial g/\partial(T^{-1})$, thus proving the correctness of eq. (12). For $Ag_{0.05}NiPS_3$ ($T = 300$–350°C) it has also been shown that the K_t versus T^{-1} curve, as determined from kinetic experiments, is a straight line with a positive slope [15].

The x-dependence of $\Delta\bar{S}_{Li}$ cannot quantitatively

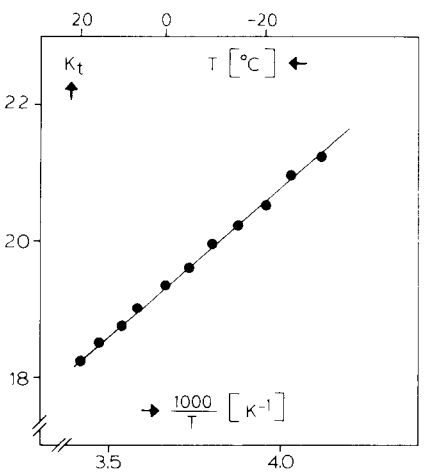

Fig. 3. The temperature dependence of the thermodynamic factor for $Li_{0.80}Ti_{1.03}S_2$, as determined from the EMF–x curves at different temperatures.

Table 1
The partial thermodynamic functions of several insertion compounds, determined from EMF-temperature measurements.

Compound	$\Delta\bar{H}_M$ (k J mole^{-1})	$\Delta\bar{S}_M$ (J mole^{-1} K^{-1})	T-range (°C)	Refs.
β-$Ag_{0.30}V_2O_5$	−16.8	+28.0	200–400	[5]
$Ag_{0.07}TiS_2$	−3.5	+30.5	150–200	[6]
$Ag_{0.01}NiPS_3$	≃−7	≃+26	200–350	[6]
$Cu_2Mo_6S_{7.59}$	≃−11.0	≃+20.7	120–170	[4]
β-$Na_{0.32}V_2O_5$	−302	−12.2	100–400	[19]
β-$Li_{0.30}V_2O_5$	−353	−24	25–50	[20]
$Li_{0.30}V_6O_{13}$	−276	−19	80–120	[21]
$Li_1V_5S_8$	−282	−84	25–40	[22]
Li_1TiS_2	−190	−28.3	25–100	[16]
$Li_{0.60}TiS_2$	−215	−14.5	25–100	[16]
$Li_{0.95}CoO_2$	−391	−51.6	−30–20	this work
$Li_{0.97}Ti_{1.03}S_2$	−189	−28.1	−30–20	this work
$Li_{0.61}Ti_{1.03}S_2$	−211	−15.1	−30–20	this work
$Li_{0.13}Ti_{1.03}S_2$	−229	−9.3	−30–20	this work

be described by eq. (14), as can be seen from fig. 2c, where the dashed line represents eq. (14). This probably indicates that the site distribution of the Li^+-ions in the Van der Waals gap deviates from what is to be expected for the stationary state; even though we have allowed for long equilibration times after the coulometric titrations. $\Delta\bar{H}_{Li}$, which more reflects the gross Coulombic interactions, is not very sensitive to the site distribution.

In table 1 the partial thermodynamic functions of several insertion compounds are summarized. The silver and copper insertion compounds exhibit the remarkable behaviour that $\Delta\bar{S}_M$ is distinctly positive. This is probably related to an exceptionally high vibrational freedom of the Ag^+, Cu^+-ions. Upon reversible and isothermal discharge, a substantial part of the electrical energy delivered by the M/M_xSSE cells (M = Ag, Cu) would be obtained from heat withdrawn from the surroundings. For the alkali insertion compounds $\Delta\bar{G}_M \simeq \Delta\bar{H}_M$, while $\Delta\bar{S}_M$ is negative. Our data for $\Delta\bar{H}_{Li}$ and $\Delta\bar{S}_{Li}$ in $Li_xTi_{1.03}S_2$ compare very well with those of Whittingham [16]. Dickens et al. [17,18] determined the enthalpy of formation of several lithium vanadium and tungsten bronzes calorimetrically. Their data for $\Delta\bar{H}_{Li}$ compare very well with the data resulting from EMF-temperature measurements. Unfortunately, no calorimetrically determined data for $\Delta\bar{H}_{Li}$ in Li_xTiS_2 are presently available.

4. The thermoelectric power in $Li_xTi_{1.03}S_2$

4.1. The electronic component of the thermoelectric power

The thermoelectric power, $\Delta E/\Delta T$, of the thermocells:

$$\underset{(T)}{\text{Pt}\,|\,Li_xTi_{1.03}S_2\,|\,\text{Pt}}\quad\underset{(T+\Delta T)}{}\qquad 0 \leqslant x \leqslant 0.97\,,$$

$$T = 50\text{–}200°C \qquad \text{(III)}$$

has been determined. The results are shown in fig. 4. The Seebeck coefficients for $Li_xTi_{1.03}S_2$ with $0 \leqslant x \leqslant 0.61$ have a positive sign (hotter electrode has a positive sign), indicating that electrons are the majority electronic charge carriers. According to Thompson [23,24] the Li_xTiS_2 materials with $x < 0.25$ can be treated in a rigid, parabolic band model. Then, the Seebeck coefficient can be written as [25]:

$$\lim_{\Delta T \to 0} (\Delta E/\Delta T) \equiv \epsilon_e \propto m^* T/n^{2/3}\,,$$

where m^* is the electron effective mass, and n the carrier concentration. Qualitatively, our measurements are in accordance with this model, as the carrier concentration is expected to increase upon insertion of lithium in TiS_2. Band structure calculations by

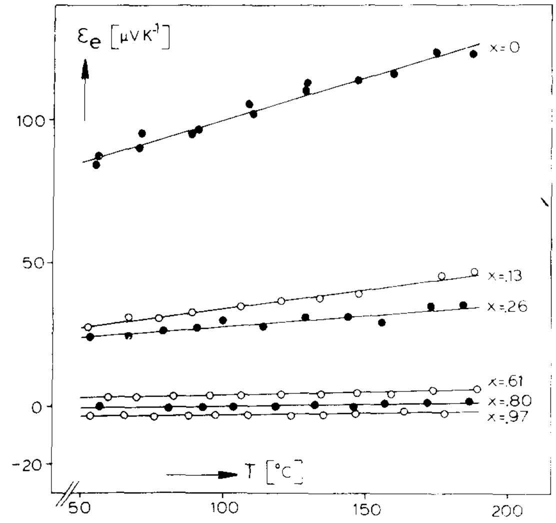

Fig. 4. The electronic Seebeck coefficient of $Li_xTi_{1.03}S_2$. The ϵ_e values have been corrected for the contribution of ϵ_{Pt}.

McCanny [26] indicate that the symmetric conduction band of Li_1TiS_2 is only half full; therefore the thermoelectric power of Li_1TiS_2 should be zero. The change of sign of the Seebeck coefficient for $x > 0.26$ might then be the result of the contribution of a non-symmetric band to the shape of the conduction band. An alternative approach to the Seebeck coefficient data for $Li_xTi_{1.03}S_2$ has been given in a previous paper [9]. However, it should be noted that for small (<50 $\mu V\ K^{-1}$) absolute values of the Seebeck coefficient, no exact calculations of the carrier concentration can be made. Then, Hall-effect measurements, which have sofar been unsuccessful for $Li_xTi_{1.03}S_2$, are indispensable.

4.2. The ionic component of the thermoelectric power

The ionic component of the thermoelectric power in $Li_xTi_{1.03}S_2$ was determined, analogous to Ag_xTiS_2 and Ag_xNiPS_3 [6,9], using thermogalvanic cells of the type:

$$\mathrm{Pt}\,|\,\mathrm{Li}\,|\,\text{electrolyte}\,|\,Li_xTi_{1.03}S_2\,|\,\text{electrolyte}\,|\,\mathrm{Li}\,|\,\mathrm{Pt}$$
$$(\longleftarrow T \longrightarrow) \qquad (\longleftarrow T+\Delta T \longrightarrow) \qquad \text{(IV)}$$

$x = 0.61, 0.80, 0.97, \quad T = -30\text{–}30°C$

electrolyte = 1 M·$LiClO_4$ in propylenecarbonate soaked onto glass-fibre paper.

The thermoelectric power for this cell is given by [27]:

$$\lim_{\Delta T\to 0}(\Delta E/\Delta T) \equiv \epsilon_{Li^+}$$
$$= F^{-1}[S^0_{Li} - \bar{S}_{Li^+} - (Q^*_{Li^+}/T)] - \epsilon_{Pt}$$
$$= -\frac{\Delta\bar{S}_{Li}}{F} - \frac{Q^*_{Li^+}}{FT} - \epsilon_{Pt}\,, \qquad (16)$$

where S^0_{Li} is the standard entropy of metallic lithium, $\bar{S}_{Li^+}$ is the partial entropy of Li^+-ions in $Li_xTi_{1.03}S_2$, $Q^*_{Li^+}$ is the heat of transport of Li^+-ions in $Li_xTi_{1.03}S_2$, and ϵ_{Pt} is the Seebeck coefficient of platinum. In eq. (16) the thermocouple effect of the Pt/Li-junctions is omitted. However, no reliable data could be obtained: $\epsilon_{Li^+} = 0 \pm 50\ \mu V\ K^{-1}$. This is probably related to the use of lithium as an electrode material. In isothermal conditions cell IV exhibits an EMF of 5–10 mV, somewhat dependent on temperature. To avoid these problems, we decided to use $Li_xTi_{1.03}S_2$ itself, as an electrode material.

For the thermogalvanic cell:

$$\mathrm{Pt}\,|\,Li_xTi_{1.03}S_2\,|\,\text{electrolyte}\,|\,Li_xTi_{1.03}S_2\,|$$
$$(\longleftarrow T \longrightarrow)$$
$$\text{electrolyte}\,|\,Li_xTi_{1.03}S_2\,|\,\mathrm{Pt}$$
$$(\longleftarrow T+\Delta T \longrightarrow) \qquad \text{(V)}$$

the thermoelectric power is given by:

$$\lim_{\Delta T\to 0}(\Delta E/\Delta T) \equiv \epsilon'_{Li^+} = -\frac{Q^*_{Li^+}}{FT} - \epsilon_{Pt}\,. \qquad (17)$$

Because $Li_xTi_{1.03}S_2$ itself is used as an electrode material, there is no entropy jump across the electrolyte. This presents one of the advantages of this novel approach: the heat of transport can be determined directly from the Seebeck coefficient. The measurements of the thermoelectric power, using thermocell V, were completely reproducible. The results for ϵ'_{Li^+} are shown in fig. 5. All Seebeck coefficients have a negative sign (hotter electrode has a negative sign), indicating that Li^+-ions are the mobile charge carriers. Also, the Seebeck coefficient decreases with increasing temperature, as is in accordance with eq. (17). The values for the heat of transport, determined directly from the

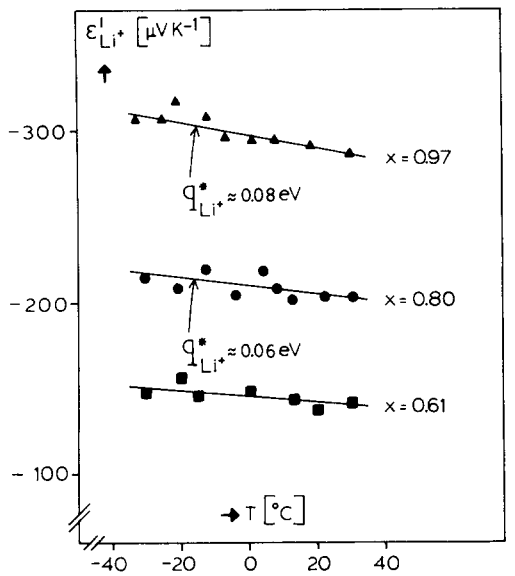

Fig. 5. The ionic Seebeck coefficient of $Li_xTi_{1.03}S_2$ (thermocell V). The ϵ'_{Li}-values have been corrected for the contribution of ϵ_{Pt}. The heat of transport ($Q^*_{Li^+}$) is determined from the slope of the ϵ'_{Li^+} versus $1/T$ curves.

Seebeck coefficient (see table 2), and determined from the slope of the Seebeck coefficient versus reciprocal temperature curves (see fig. 5) compare reasonably well, proving the correctness of the applied method. With the data for $Q^*_{Li^+}$, determined from the Seebeck coefficient data (ϵ'_{Li^+}) of thermocell V, and $\Delta\bar{S}_{Li}$, resulting from EMF-temperature measurements (see section 3.2), the Seebeck coefficient (ϵ_{Li^+}) of thermocell IV, can be calculated. The results of this calculation are shown in table 2, from which it can be seen that despite the difficulties associated with the use of lithium as an electrode material, the experimental data for ϵ_{Li^+} (thermocell IV) are in rough correspondance with the calculated ones.

The theoretical importance of the heat of transport follows from the comparison of this quantity with the activation enthalpy for ionic conduction (ΔH_{act}, σ_{Li^+}). Because the exact determination of ΔH_{act}, σ_{Li^+} is a time consuming process, we determined the activation enthalpy for the average chemical diffusion coefficient in $Li_xTi_{1.03}S_2$ ($\Delta H_{act} - \widetilde{D}_{av,Li^+}$) using a fast electrochemical method [11]. Also, it has been shown [15], for $Ag_{0.05}NiPS_3$, that when the thermodynamic factor decreases and the chemical diffusion coefficient increases with increasing temperature ΔH_{act}, $\sigma_{Li^+} > \Delta H_{act}$, $\widetilde{D}_{Li^+}$. Because $\Delta H_{act} - \widetilde{D}_{av,Li^+} = 0.48$ eV it follows that ΔH_{act}, $\sigma_{Li^+} \gg Q^*_{Li^+}$ for the $Li_xTi_{1.03}S_2$ materials. This phenomenon has also been observed for Ag_xTiS_2 with $0 < x < 1$ and $Ag_{0.05}NiPS_3$ [6,9]. According to the "extended lattice gas model" of Girvin [10], ΔH_{act}, σ_{M^+} is composed of a static and dynamic part, W and $E_b/2$, respectively. For the Ag_xSSE and $Li_xTi_{1.03}S_2$ materials the heat of transport equals the static part, while the cation–anion interaction (Ag^+, Li^+, $\Leftrightarrow S^{2-}$) results in a major contribution to the ionic polaron binding energy (E_b). This is in contrast with several ideal fast ionic conductors, like AgI [28], the AgI-based electrolytes [29], and β, β''-alumina [30], where the lattice disorder is very high and the heat of transport equals the activation enthalpy for ionic conduction. Unfortunately, no data on the heat of transport of lithium ion conductors are available form literature to date.

Table 2
Data related to the ionic component of the thermoelectric power in $Li_xTi_{1.03}S_2$.

$x(Li_xTi_{1.03}S_2)$	$Q^*_{Li^+}$ (eV) (thermocell V)	$-\frac{Q^*_{Li^+}}{FT}$ (μV K^{-1}) (T = 20°C)	$\Delta\bar{S}_{Li}$ (J mol^{-1} K^{-1})	$-\frac{\Delta\bar{S}_{Li}}{F}$ (μV K^{-1})	ϵ_{Li^+} (μV K^{-1}) (thermocell IV) calc.
0.97	0.080	−273	−28.1	+291	+18
0.80	0.057	−195	−25.2	+261	+66
0.61	0.039	−133	−15.1	+157	+24

5. A comparison of some kinetic thermodynamic and thermoelectric properties of Ag_xTiS_2 and $Li_xTi_{1.03}S_2$

In ref. [11] we compare the variation of the chemical diffusion coefficient of the cation (Li^+) in $Li_xTi_{1.03}S_2$ and Li_xCoO_2 with the amount of intercalated Li^+, and thus with the changes in the c-axis. Here we also want to compare the thermodynamic and thermoelectric properties. Unfortunately, we do not have data on the ionic heat of transport for Li_xCoO_2. Therefore we will discuss the trends by comparing all available data for $Li_xTi_{1.03}S_2$ [11] and Ag_xTiS_2 [6,9,15]. This also enables us to reduce the problem to the difference in the two cations, intercalated in the same layered structure. However, we should bare in mind that the details of the structures may differ slightly. For the general discussion we think that these differences are of no consequence.

For both mentioned insertion compounds we observe an increasing c-axis with increasing x [24,32]. This is the logical result of the donation of electrons by the inserted element to the d_{z^2} orbitals of Ti^{4+}, as was discussed in [11]. However, for $\tilde{D}_{M^+}$, $Q^*_{M^+}$ and $\Delta\bar{S}_M$ we observe an opposite behaviour for both materials, as can be seen in fig. 6. While for the Li compound the entropy of dissolution behaves normally, with a negative value in the whole x-range, and decreases to more negative values with increasing x, the entropy of dissolution is positive for the Ag compound as we have already discussed in this paper (see fig. 2c). The reason for this positive value of $\Delta\bar{S}_{Ag}$ is the high degree of vibrational freedom of the Ag^+-ions in the

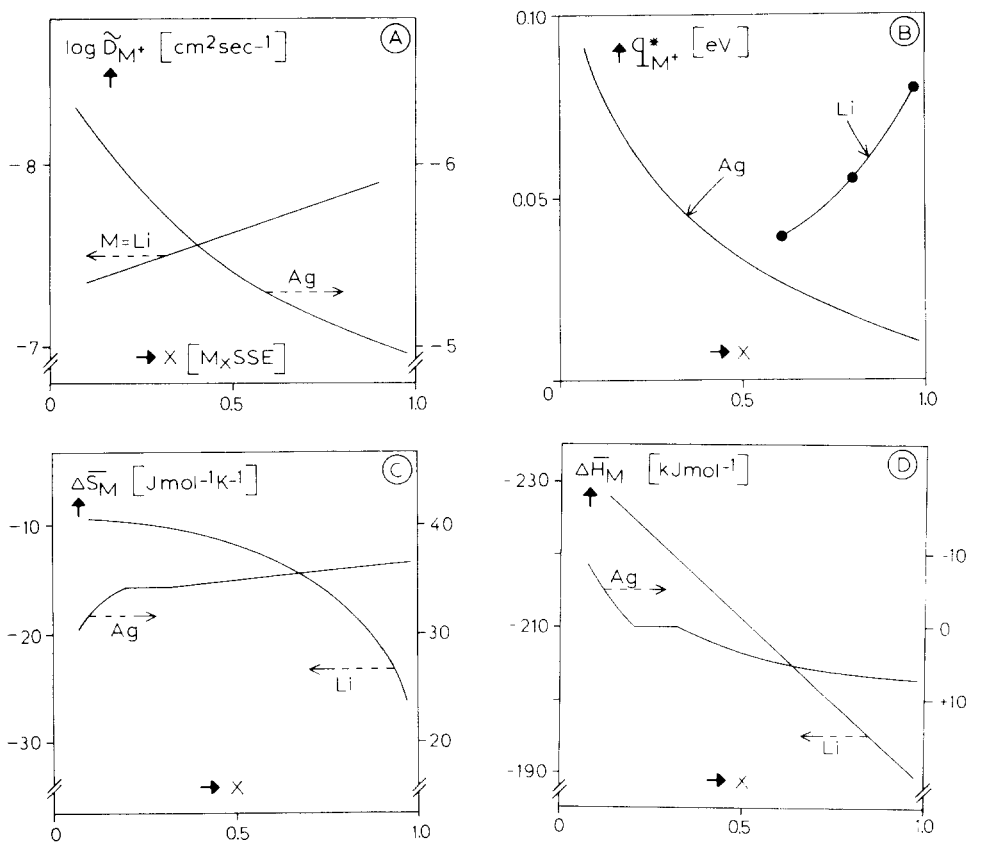

Fig. 6. The x-dependence of the chemical diffusion coefficient ($\tilde{D}_{M^+}$), the ionic heat of transport ($Q^*_{M^+}$), and the partial thermodynamic functions ($\Delta\bar{H}_M$ and $\Delta\bar{S}_M$) of Ag_xTiS_2 and $Li_xTi_{1.03}S_2$. $\tilde{D}_{Ag^+}$ for T = 193°C – $Q^*_{Ag^+}$, $\Delta\bar{H}_{Ag}$, $\Delta\bar{S}_{Ag}$ for T = 150–200°C, $\tilde{D}_{Li^+}$ for T = 20°C – $Q^*_{Li^+}$, $\Delta\bar{H}_{Li}$, $\Delta\bar{S}_{Li}$ for T = –30–30°C.

Van der Waals gap. This entropy of dissolution increases with x, which can be expected for the rather disorganized structure that results from insertion of Ag^+-ions within the Van der Waals gap formed by S^{2-}-ions that have a high polarizability like the Ag^+-ions. Insertion of the smaller Li^+-ions results in a further ordening of the S^{2-}-ions around the Li^+-ions with higher values of x. This higher degree of order is also reflected in the decreasing value of $\widetilde{D}_{Li^+}$ with x (see fig. 6a). Also the tendency of $Q^*_{Li^+}$, the ionic heat of transport, to increase with increasing x (see fig. 6b) confirms the decreasing disorder, because the heat of transport reflects the excess entropy of a selected ensemble of mobile Li^+-ions. When the disorder is high, nearly all the Li^+-ions contribute, or in other words: hardly any selection takes place. Thus for higher values of x we expect higher values of $Q^*_{Li^+}$ if the material is further ordered. For the Ag compound we observe the opposite tendency, not only in the peculiar behaviour of the entropy of dissolution, but also in the increasing values of $\widetilde{D}_{Ag^+}$ with increasing x and in the decreasing values of $Q^*_{Ag^+}$ with increasing x as can be observed in figs. 6a and 6b. A higher amount of inserted Ag^+-ions results in more disorder (vibrational freedom) which is reflected in the lower value for $Q^*_{Ag^+}$ and the decreasing $\widetilde{D}_{Ag^+}$. The enthalpy of dissolution of the Li and Ag compounds is given in fig. 6d. Both increase with increasing x, as may be expected, since the enthalpy reflects the overall electrostatic interaction of the positive ions in the Van der Waals gap. Higher concentrations result in more repulsion between the inserted ions themselves. Moreover, we can observe that $\Delta\bar{H}_M$ for the Li compound has much lower (more negative) values than for the Ag compound, as a result from the high polarizing power of the small Li^+-ion. $\Delta\bar{H}_{Ag}$ even gets positive values (though very small!) for high values of x, which means that Ag_xTiS_2 for high values of x can only exist thanks to its extremely high positive entropy of dissolution.

6. The electronic component of the thermoelectric power in Li_xCoO_2 in relation to the stability of this material

The thermoelectric power, $\Delta E/\Delta T$, of the thermocells:

$$\underset{(T)}{Au}\,|\,Li_xCoO_2\,|\,\underset{(T+\Delta T)}{Au}$$

$$x = 0.20, 0.60, 0.80, 1.00,\ T = 30\text{–}400^\circ C \quad \text{(VI)}$$

has been determined. In fig. 7 the dependence on x and temperature of the (electronic) Seebeck coefficient is depicted, while fig. 8 shows the cycling behaviour of the Seebeck coefficient for two typical materials. The Seebeck coefficients for Li_xCoO_2 have a negative sign (hotter electrode has a negative sign), indicating that electron holes are the majority electronic charge carriers.

Thermogravimetric analysis indicates that the Li_xCoO_2 materials with $x < 1$ decompose into Li_1CoO_2 and Co_2O_3, whilst releasing oxygen, in the temperature range 80–500°C. The corresponding DTA-runs indicate that this reaction is weakly exothermic. A typical thermogram is shown in fig. 9. Finally, in the temperature range 950–1050°C decomposition into Li_2O and Co_3O_4 takes place. The decomposition products were also positively identified with X-ray diffraction.

In fig. 7 and also in figs. 8 and 9 we can clearly observe that Li_xCoO_2 is only stable in a very narrow composition range. The lower limit for x is $\simeq 0.94$, as we determined with kinetic experiments [11]. For Li_1CoO_2 we find reasonally high absolute values for the Seebeck coefficient (ϵ_h) in the whole temperature range from 30–400°C. This, together with the negative sign of ϵ_h, suggests that the electrical transport takes place through moving electron holes in a Co^{3+} valence band. In fact a very small deviation from $x = 1$, e.g. 0.998, would result effectively in 2‰ Co^{4+} sites. However, at concentrations of Co^{4+} above some % we may expect strong interaction between the electron holes, and a non-ideal behaviour. This also implies that the Co^{4+} lattice sites do approach each other (for decreasing x-values), thereby reducing the structural stability of the material, since Co^{4+} can only exist in a diluted solution in a $\{Co^{III}Li^{I}\}$ oxide lattice. CoO_2 as such is not stable [31] and would decompose into Co_2O_3 and oxygen. Structural data on Li_xCoO_2 were discussed in a previous paper [11]. Here, we only want to recall that the c-axis perpendicular to the oxygen layers decreases with increasing x. The stability of the structure thereby increases with x. Without Li^+-ions between the oxygen layers, two reasons for the instability of the resulting "CoO_2" structure can be mentioned: first a for-

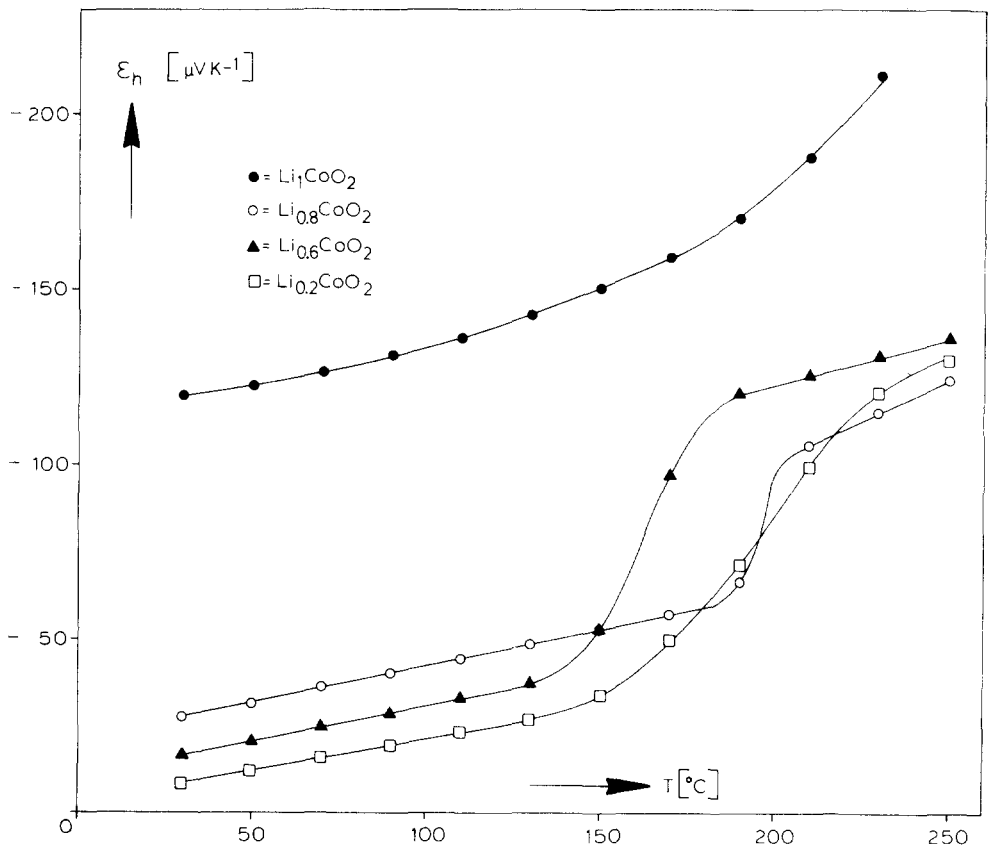

Fig. 7. The electronic Seebeck coefficient of Li_xCoO_2. The ϵ_h values have been corrected for the contribution of ϵ_{Au}.

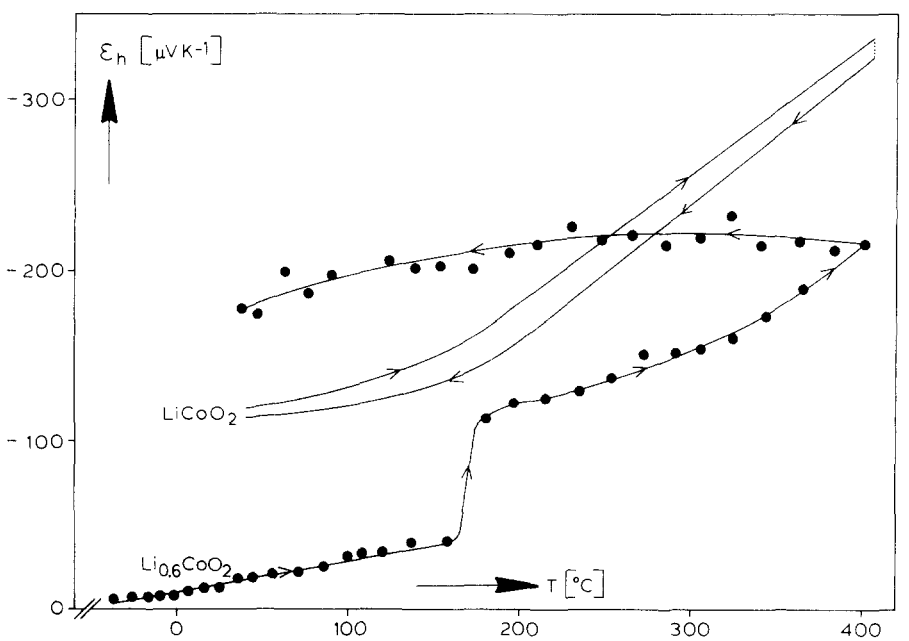

Fig. 8. Cycling behaviour of the electronic Seebeck coefficient of Li_xCoO_2.

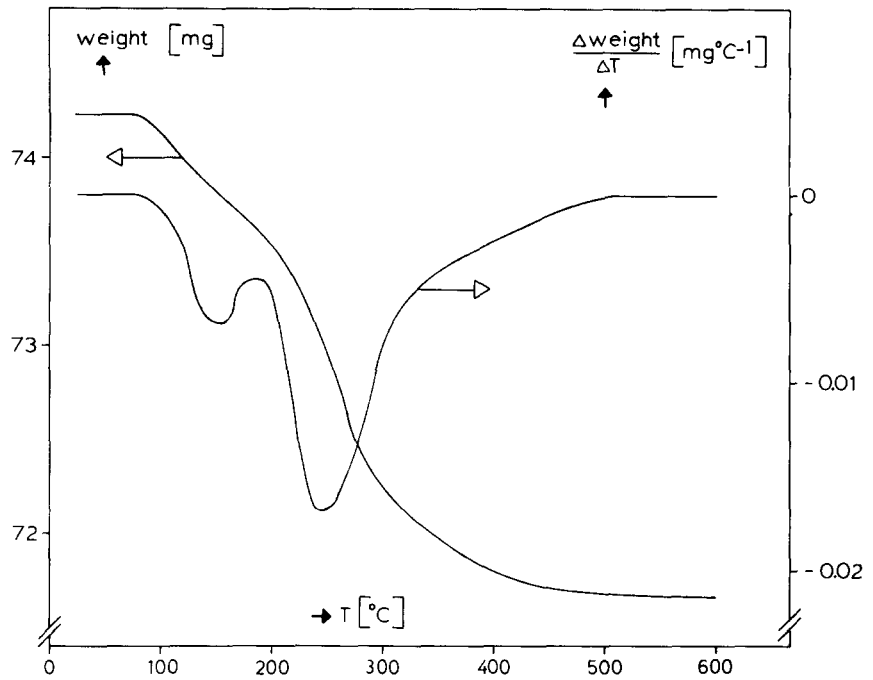

Fig. 9. Thermogram of $Li_{0.57}CoO_2$ atmosphere: oxygen; heating rate: 5°C min^{-1}.

mal overall valency of 4^+ for Co is quite extraordinary, and second the O^{2-}-ions in the two layers around the Van der Waals gap would result in very strong repulsive forces, since the O^{2-}-ion is not very well polarizable. Therefore, we can expect that the electrical conductivity of Li_xCoO_2 increases while ϵ_h decreases when x decreases from 1.00 to about 0.94. At lower values of x the Seebeck coefficient hardly changes anymore, as can be clearly observed in fig. 7. The absolute differences between the ϵ_h-values for x = 0.80, 0.60 and 0.20 are relatively small, due to the non-ideal behaviour. Also, the increase in the electrical conductivity with decreasing x is less than expected. Moreover, we think that these materials do only exist below 80°C due to the fact that the decomposition to Li_1CoO_2 and Co_2O_3 is retarded kinetically. The formation of a critical nucleus of the new phase with a different structure obviously cannot take place at these lower temperatures. The rather slow weight loss starting at around 125°C, as is observed in the thermogram in fig. 9, together with the faster increase in reaction rate observed at 250°C point into the same direction. The reaction rate between 125°C and 250°C is very much influenced by nucleation processes, while above 250°C only growth of the newly formed phase is observed. In figs. 7 and 8 we can observe that above 150°C decomposition takes place, resulting in a much higher Seebeck coefficient, which now reflects the properties of the mixture of Li_1CoO_2 and Co_2O_3. Of course this process is irreversible as can be clearly seen in fig. 8.

References

[1] P. Vashishta, J.N. Mundy and G.K. Shenoy, eds., in: Fast ion transport in solids (North-Holland, Amsterdam, 1979).
[2] J.B. Bates and G.C. Farrington, eds., in: Fast ionic transport in solids (North-Holland, Amsterdam, 1981).
[3] M. Kleitz, ed., in: Fast ionic transport in solids (North-Holland, Amsterdam, 1983).
[4] G.J. Dudley, K.Y. Cheung and B.C.H. Steele, J. Solid State Chem. 32 (1980) 269.
[5] B.B. Scholtens, R. Polder and G.H.J. Broers, Electrochim. Acta 23 (1978) 483.
[6] A. Honders, A.J.H. Hintzen, E.W.A. Young, J.H.W. de Wit and G.H.J. Broers, Solid State Ionics, accepted for publication.

[7] M.B. Armand, Thesis (Grenoble, 1978).
[8] A. Honders, E.W.A. Young, J.H.W. de Wit and G.H.J. Broers, Solid State Ionics 8 (1983) 115.
[9] A. Honders, A.J.H. Hintzen, J.M. der Kinderen, J.H.W. de Wit and G.H.J. Broers, Solid State Ionics 9/10 (1983) 1205.
[10] S.M. Girvin, J. Solid State Chem. 25 (1978) 65.
[11] A. Honders, J.M. der Kinderen, A.H. van Heeren, J.H.W. de Wit and G.H.J. Broers, Solid State Ionics, submitted for publication.
[12] A. Honders and J.H.W. de Wit, J. Appl. Electrochem. 10 (1980) 409.
[13] A. Honders, E.W.A. Young, A.H. van Heeren, J.H.W. de Wit and G.H.J. Broers, Solid State Ionics 9/10 (1983) 375.
[14] K. Cheung, B.C.H. Steele and G.J. Dudley, in: Fast ion transport in solids, eds. P. Vashishta, J.N. Mundy and G.K. Shenoy (North-Holland, Amsterdam, 1979).
[15] A. Honders, E.W.A. Young, A.J.H. Hintzen, J.H.W. de Wit and G.H.J. Broers, Solid State Ionics, submitted for publication.
[16] M.S. Whittingham, Progr. Solid State Chem. 12 (1978) 41.
[17] P.G. Dickens, S.J. French, A.T. Hight, M.F. Pye and G.J. Reynolds, Solid State Ionics 2 (1981) 27.
[18] P.G. Dickens and S.A. Kay, Solid State Ionics 8 (1983) 291.
[19] B.C.H. Steele, in: Mass transport phenomena in ceramic eds. A.R. Cooper and A.H. Heuer (Plenum Press, New York, 1975) p. 269.
[20] A.V. Popov, Y.G. Metlin and Y.D. Tretyakov, J. Solid State Chem. 32 (1980) 343.
[21] P.C. Spurdens, J. Drennan, J.R. Owen, J.M. Gonzales-Calbet and D.A. Jefferson, Solid State Ionics 5 (1981) 335.
[22] F. Dalard, D. Deroo, A. Sellami, R. Mauger and J. Mercier, Solid State Ionics 7 (1982) 17.
[23] A.H. Thompson, Phys. Rev. Letters 35 (1975) 1786.
[24] A.H. Thompson and C.R. Symon, Solid State Ionics 3/4 (1981) 175.
[25] E.M. Logothetis, W.J. Kaiser, C.A. Kukkonen, S.P. Faile, R. Colella and J. Gambold, Physica 99B (1980) 193.
[26] J.V. McCanny, J. Phys. C12 (1979) 3263.
[27] C. Wagner, Progr. Solid State Chem. 7 (1972) 1.
[28] H. Shahi and S. Chandra, Z. Naturforsch. 30A (1975) 1055.
[29] K. Shahi, Phys. Status Solidi 41A (1977) 11.
[30] H. Kuwamoto and H. Sato, Solid State Ionics 5 (1981) 187.
[31] G.W. Simmons, A. Vertes, M.L. Varsányi and U. Leidheiser Jr., J. Electrochem. Soc. 126 (1979) 187.
[32] G.A. Scholtz, R.F. Frindt, Mat. Res. Bull. 15 (1980) 1701.